J. Fluid Mech. (2026), *vol.* 1030, R5, doi:10.1017/jfm.2026.11308

JFM RAPIDS

Spreading versus non-spreading of wetting films: enhancing aqueous phase invasion in disordered media via nanoparticle adsorption

Xukang Lu[1], **Mingbao Zhang**[1], **Wenhai Lei**[2], **Yang Liu**[1,3], **Yueyang Yu**[1], **Tianzhu Jiang**[1] and **Moran Wang**[1,4]

[1]Department of Engineering Mechanics, Tsinghua University, Beijing 100084, PR China

[2]Department of Engineering Mechanics, KTH Royal Institute of Technology, Stockholm 100 44, Sweden

[3]Spanish National Research Council (IDAEA-CSIC), Barcelona 08034, Spain

[4]Department of Mechanical Engineering, Johns Hopkins University, Baltimore, MD 21218, USA

Corresponding author: Moran Wang, moralwang@jhu.edu; mrwang@tsinghua.edu.cn

(Received 24 October 2025; revised 12 December 2025; accepted 10 February 2026)

Controlling multiphase flow in disordered media is central to diverse practical contexts. Although nanoparticles have been widely utilised to modify surface wettability, factors governing their effects on dynamic displacement patterns remain unclear. Here, we identify the criterion for nanoparticle-induced wettability alteration during displacement by combining interfacial-scale wetting models, pore-scale microfluidic experiments and simulations. Motivated by striking contrasts in static wettability, we find that nanoparticle adsorption on solid surfaces affects displacement interfaces only when spreading of wetting films is pre-established, corresponding to corner-flow conditions. Displacement experiments under varying intrinsic wettability show that wetting-film development and non-aqueous droplet detachment are strengthened exclusively on moderately water-wet surfaces satisfying the corner-flow criterion. Investigations across designed porous structures with varying degrees of structural hierarchy validate the generality of the wettability criterion, while improvement in displacement efficiency diminishes with reduced hierarchy. The structural effect arises from variations in flow heterogeneity, with stronger heterogeneity simultaneously promoting film flow and ganglion mobilisation. The coupled impacts of wettability and structural conditions are summarised in an illustrative phase diagram delineating nanoparticle-tuned multiphase displacement. Our findings offer mechanistic insights into complex fluid flow in porous media and suggest optimised strategies for displacement control via nanoparticle suspensions.

Key words: porous media, suspensions

---

1. Introduction

Multiphase flow in porous media is widely encountered in a broad range of natural and industrial scenarios, including but not limited to geological carbon sequestration (Huppert & Neufeld 2014), soil remediation (Pak *et al.* 2020), hydrocarbon recovery (Blunt 2017) and engineering cellular fluidics (Dudukovic *et al.* 2021). Dynamics of multiphase flow can be strongly influenced by complex fluids, such as polymers (Browne *et al.* 2023), surfactants (Sundin & Bagheri 2022) and particle suspensions (Qin *et al.* 2023). Among these, nanoparticles have drawn particular attention owing to pronounced interfacial effects. Extensive efforts have been made to understand how nanoparticle adsorption at solid surfaces (Al-Anssari *et al.* 2016), adsorption at liquid–liquid interfaces (Xu *et al.* 2017) and ordering in the thin-film region (Wasan & Nikolov 2003) modify interfacial properties. Notably, solid surface adsorption of nanoparticles has been reported to drastically alter surface wettability (Al-Anssari *et al.* 2016), a critical factor influencing multiphase flow (Zhao, MacMinn & Juanes 2016). However, performance evaluations and interpretations were largely based on *ex situ* characterisations, leaving the unique roles of interfacial evolution and geometric variations poorly understood.

When and how can nanoparticles reshape multiphase flow in porous media? On the one hand, static characterisations have shown pronounced inconsistencies in nanoparticle-induced wettability variations depending on measurement conditions (Lim *et al.* 2015; Al-Anssari *et al.* 2016; Alzobaidi *et al.* 2021), yet the underlying factors and the correspondence between static and dynamic interfacial states have not been well discussed. On the other hand, in flow experiments applying nanoparticle suspensions, significant impacts on displacement patterns were predominantly reported under hydrophilic rather than hydrophobic conditions (Zhang *et al.* 2018; Mohammadalinejad *et al.* 2019). The mechanisms governing such transitions from efficient to inefficient displacement are highly debated (Zhang *et al.* 2018; Lei *et al.* 2025). Furthermore, the relative improvement in displacement efficiency varied greatly across natural sand packs (Zhang *et al.* 2016), heterogeneous micromodels (Lu & Wang 2023) and regular micromodels (Li *et al.* 2017), while the dominant displacement modes and the origin of structural effects remain unclear. Overall, existing studies suggest limited scenarios for nanoparticle effects on displacement processes, while quantitative criteria based on fluid mechanical insights are lacking.

In this work, we uncover the mechanisms governing nanoparticle-induced wettability alteration during displacement through multiscale experiments and analysis. At the interfacial scale, we reveal contrasts in the effectiveness of wettability alteration under different set-ups by experimental characterisation and theoretical analysis of interfacial properties and adsorption behaviours, highlighting the critical role of film spreading for displacement conditions. At the pore scale, we validate the generality of the proposed wettability criterion, identify the dominant displacement mode, and demonstrate how the structural hierarchy modulates displacement enhancement by microfluidic experiments and simulations. Together, these insights yield a phase diagram integrating wettability and structural effects, providing a mechanistic basis for controlling multiphase flow in disordered media via nanoparticle adsorption on solid surfaces.

2. Methods

Nanoparticle suspensions (concentration 1 wt. %, nominal diameter 20 nm) were prepared by diluting stock silica sol (Nissan Chemical) with deionised water. The hydrophilic silica nanoparticles caused negligible change in interfacial tension σ (from $49.3 \pm 0.6\,\mathrm{mN\,m^{-1}}$ to $47.8 \pm 0.4\,\mathrm{mN\,m^{-1}}$), indicating a weak tendency to adsorb at the liquid–liquid interface. Moreover, owing to the low concentration, particle ordering in the three-phase contact region and the associated structural disjoining pressure effects (Wasan & Nikolov 2003) can be safely ignored. Brine of the same pH and salinity was formulated for comparison. The non-aqueous phase liquid (NAPL) was n-decane (95 %, Macklin), fluorescently dyed with Nile Red (100 ppm, Macklin) for microfluidic visualisation.

Wettability characterisations were performed by measuring the apparent contact angle θ_{eff} under two representative configurations. For a NAPL droplet in an aqueous environment, cleaned substrates were immersed in the aqueous phase (brine or nanoparticle suspension) for 1 h before placing a 5 μL droplet. For an aqueous droplet in a NAPL environment, substrates were instead immersed in the non-aqueous phase without suspension treatment, and the droplet (brine or nanoparticle suspension) was then deposited in a rapid (within seconds) and gentle manner, to minimise effects from contact line receding. The intrinsic wettability for the brine/NAPL/substrate system, θ_w, was varied using different materials: piranha-treated silica (moderately water-wet, $\theta_w \approx 36^\circ$), untreated silica (weakly water-wet, $\theta_w \approx 52^\circ$) and untreated silicon (nearly neutral, $\theta_w \approx 87^\circ$). Note that reported values are from sessile drop measurements. The contact angle hysteresis, evaluated by the difference between advancing and receding angles, was below 5° under the water-wet conditions and below 10° under the nearly neutral condition, indicating limited pinning effects. Microscopic adsorption states were further examined by scanning electron microscopy (SEM). The treated substrates were withdrawn from the suspension, gently rinsed, dried in air and carbon-coated. The obtained images were filtered and binarised, and the surface coverage of particles was quantified by $\alpha = N\pi d_p^2/(4A_0)$, where N is the particle number identified by watershed segmentation, d_p is the nominal diameter, and A_0 is the total surface area. At least three independent images were counted for statistics.

Three disordered porous structures were designed and generated using the Quartet Structure Generation Set (QSGS) method (Wang *et al.* 2007), which is further improved here to produce controllable complexity while avoiding connectivity issues. Using a two-step generation strategy, the degree of structural hierarchy was tuned by adjusting the ratio of larger to smaller grains under constant porosity ($\phi = 40\,\%$). The resulting 2D pore size distributions ranged from long-tailed to nearly Gaussian, reflecting geometric variations in natural media that induce structural and flow heterogeneity (Wong, Koplik & Tomanic 1984). Single-phase network modelling (Liu *et al.* 2022) was employed to provide a quantitative measure of heterogeneity. Lattice Boltzmann simulations were also performed to visualise detailed velocity fields. Details of the improved QSGS method, set-up and pore-scale simulations are provided in the supporting information.

Microfluidic chips were fabricated from silicon using standard photolithography and dry-etching techniques. By using original, thermally oxidised and piranha-treated thermally oxidised silicon wafers, channel surfaces with varying wettability as in static characterisations were obtained. For displacement experiments, the porous medium was first saturated with dyed oil, after which the aqueous phase was injected. The capillary number $Ca_m = \mu U_m/\sigma$ was controlled at 2.6×10^{-6}, where μ is the viscosity of the invading fluid and $U_m = Q_{in}/(WH\phi)$ is the characteristic velocity, with Q_{in} the injection rate, W the total width (6 mm) and H the chip depth (40 μm). With a water-to-oil viscosity ratio of approximately 1.2, viscous instability is negligible. Each experiment was repeated three times. Image processing was performed based on binarisation from fluorescence imaging.

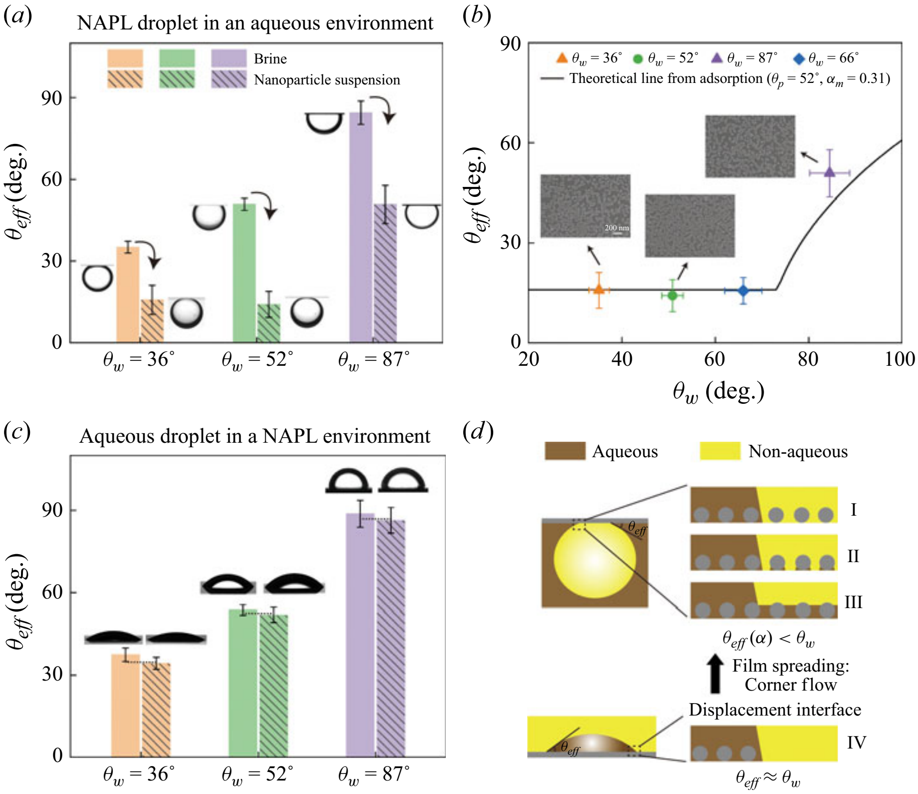

Figure 1. Static characterisation and analysis of wettability variations. (*a*) Variations in the apparent contact angle θ_{eff} of the aqueous phase in NAPL droplet systems. Substrates with intrinsic wettability θ_w ranging from 36° to 87° were immersed in either brine or nanoparticle suspensions for 1 h before depositing a non-aqueous droplet. Insets show droplets exhibiting different apparent wettability. (*b*) Theoretical validation of the relationship between solid surface adsorption and apparent wettability change, where α_m is the surface coverage averaged from SEM and θ_p is the intrinsic wettability of nanoparticles. An additional condition was validated near the turning point, where the silica surface was modified using 3-aminopropyl-triethoxysilane to achieve $\theta_w \approx 66^\circ$. Insets show representative SEM images. (*c*) Variations in θ_{eff} in aqueous droplet systems. Substrates were immersed in the non-aqueous phase before depositing an aqueous droplet. Insets show corresponding droplet profiles. (*d*) Schematics of distinct wetting states and nanoparticle adsorption conditions for the two configurations.

3. Results and discussion

3.1. *Experimental characterisations of static wettability and theoretical analysis*

Wettability characterisations were first performed under static conditions. The plate-based measurements aim to quantify the intrinsic solid–fluid affinity, providing general insights into the intrinsic wettability dependence of nanoparticle effects. As shown in figure 1(*a*), for NAPL droplets, nanoparticles consistently shifted the apparent wettability toward more hydrophilic states under all conditions. Under moderately and weakly water-wet conditions, the aqueous phase contact angle θ_{eff} of nanoparticle suspensions both decreased to $\sim 15^\circ$, corresponding to a strongly water-wet state.

Several microscopic phase states can exist between the non-aqueous droplet and the nanoparticle-modified substrate: the wetting phase surrounding adsorbed particles is either depleted (state I), retained between particles and the substrate (state II) or stabilised among neighbouring particles (state III). Constrained by intrinsic wettability at the surfaces, the corresponding contact angles can be derived by extending classical wetting models (Quéré 2008), given by $\cos\theta_I = \cos\theta_w + 4\alpha\cos\theta_p$, $\cos\theta_{II} = \cos\theta_I + 2\alpha\cos\theta_p(1 - \sin\theta_w/\sin\theta_p)$ and $\cos\theta_{III} = -\alpha(\cos\theta_p - 1)^2 + 1$, where α is the projected surface coverage, and θ_p and θ_w are intrinsic contact angles of the particle and wall surfaces, respectively. The thermodynamically stable state corresponds to the largest contact angle for the surrounding phase, giving $\theta_{eff} = \max(\theta_I, \theta_{II}, \theta_{III})$. Detailed derivations are provided in the supporting information. To clarify the role of solid surface adsorption, treated substrates were characterised using SEM. Similar monolayer structures and adsorption capacities were observed across the substrates after 1 h of suspension treatment (insets of figure 1*b*), with only minor variations in surface coverage and an average coverage of $\alpha_m = 0.31 \pm 0.05$ (standard deviation over all conditions). Substituting α_m and θ_p (unmodified silica nanoparticles, $\theta_p = 52^\circ$) into the expression for θ_{eff}, the relationship between θ_{eff} and θ_w can be predicted theoretically. The good agreement between theoretical and experimental results (figure 1*b*) quantitatively confirm that nanoparticle adsorption on solid surfaces drives the wettability changes.

In a three-phase system, static wettability can be characterised under two configurations, depending on which phase is defined as the droplet phase. In principle, phase configuration should not strongly affect measured wettability, as it intrinsically reflects the interfacial property. However, as shown in figure 1(*c*), nanoparticles produced negligible changes in θ_{eff} for aqueous droplets. The variations fell mostly within experimental uncertainty, indicating that nanoparticle adsorption became ineffective.

What causes the transition from significant to negligible wettability alteration? Figure 1(*d*) illustrates microscopic interfacial states under different configurations. In the NAPL droplet system, the surface is initially occupied by the aqueous phase, and the droplet deposition follows a drainage process. Nanoparticle adsorption occurs symmetrically on both sides of the liquid–liquid interface, increasing the energy difference and thereby decreasing θ_{eff}, as detailed in contact angle derivations. In the aqueous droplet system, adsorption is limited inside the droplet. Substituting the asymmetric adsorption states into the energy balance yields $\cos\theta_{eff} = \cos\theta_w - 4\alpha\sigma_{NP}/\sigma < \cos\theta_w$, where σ_{NP} denotes the water–nanoparticle interfacial energy. This predicts $\theta_{eff} > \theta_w$, inconsistent with our observations. The contradiction arises because θ_{eff} should depend only on variations in properties at the contact line (Shardt & Elliott 2020). For confined adsorption within the droplet, the contact-line region is barely affected, even though the total energy on the aqueous side is substantially modified. Consequently, the thermodynamic state of the interface remains nearly unchanged, yielding $\theta_{eff} \approx \theta_w$. The discrepancies in nanoparticle-induced wettability variations in earlier studies are also rationalised by the analysis documented earlier: significant wettability alteration from oil-wet to water-wet was observed predominantly for NAPL droplets (Al-Anssari *et al.* 2016; Alzobaidi *et al.* 2021), whereas relatively minor contact angle changes were reported for aqueous droplets (Lim *et al.* 2015).

Inspired by the striking contrasts in static wettability, we revisit nanoparticle effect on wettability under flow conditions. Evolution of the displacement interface closely resembles the configuration for aqueous droplets, with the pore space initially occupied by the non-aqueous phase. Nanoparticle adsorption lags interfacial propagation and can modify only surfaces already in contact with the aqueous phase. Therefore, wettability alteration requires pre-existing wetting films that allow nanoparticles to access NAPL-occupied surfaces (figure 1*d*) and break the interfacial equilibrium. For an isolated droplet on a smooth substrate, this is difficult unless complete wetting occurs. For microflow systems, spontaneous corner flow provides a feasible way for pre-spreading of wetting

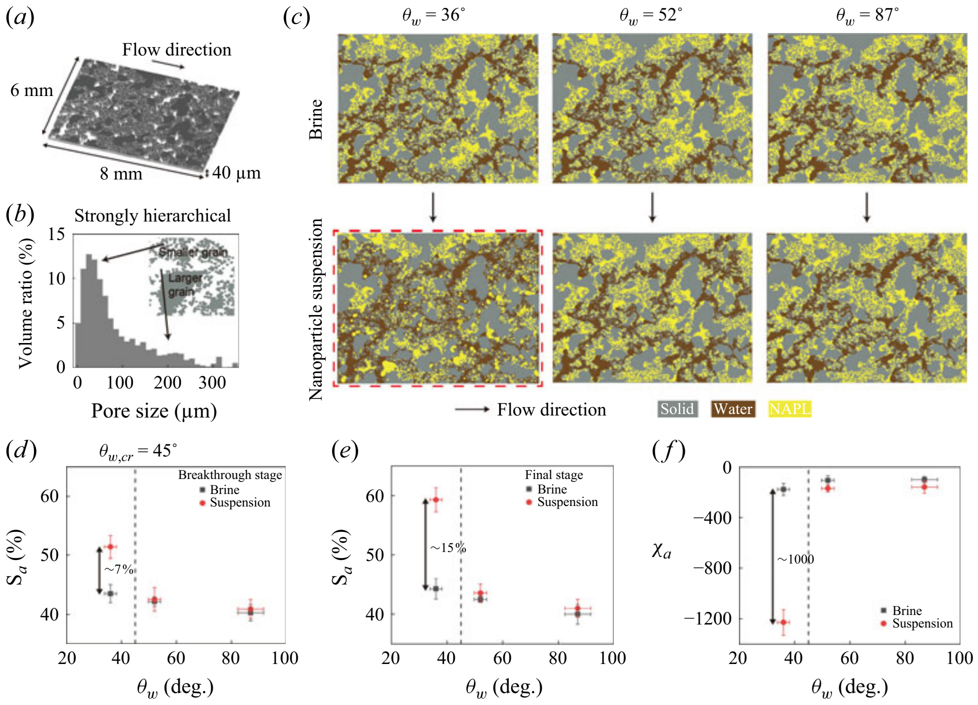

Figure 2. Validation of the wettability criterion for displacement in a strongly hierarchical disordered medium by microfluidic experiments. (*a*) Schematic of the porous structure with grey indicating solid and white indicating pore space. (*b*) Long-tailed pore size distribution. Inset: top-down view of a local structure with hierarchical features; arrows indicate smaller and larger pores. (*c*) Comparison of final phase distributions. Significant changes occurred only under the moderately water-wet condition ($\theta_w = 36^\circ$). (*d,e*) Variations in the aqueous phase saturation S_a at the (*d*) breakthrough and (*e*) final stages versus θ_w. (*f*) Variation in the Euler number of the aqueous phase χ_a versus θ_w. Dashed lines in (*d–f*) denote the wettability criterion ($\theta_w < \theta_{w,cr}$).

films, with the criterion given by $\theta_w < 90^\circ - \beta/2$, where β is the corner angle (Concus & Finn 1969). For etched microchannels, the corners are always right-angled ($\beta = 90^\circ$), thus $\theta_w < \theta_{w,cr} = 45^\circ$, serving as the criterion for nanoparticle-induced wettability alteration during displacement.

3.2. *Displacement performance and mechanisms in a disordered medium*

To validate the wettability criterion, displacement experiments were performed in a disordered medium with complex pore geometry (figures 2*a* and 2*b*). As presented in figure 2(*c*), nanoparticle suspensions produced significant changes in phase distribution relative to brine only when the corner-flow criterion was satisfied (moderately water-wet, $\theta_w = 36^\circ$). The invading pattern became more compact with increased branching, corresponding to a more water-wet state. Figures 2(*d*) and 2(*e*) show substantial increases in aqueous phase saturation S_a when $\theta_w < \theta_{w,cr}$, which expanded after breakthrough. In contrast, variations in S_a were negligible under the weakly water-wet and nearly neutral conditions, where corner flow was inhibited. Differences in material properties other than intrinsic wettability cannot explain these observations, as adsorption capacities on the substrates were similar (figure 1*b*). As shown in figure 2(*f*), the pronounced reduction in the total Euler number of the aqueous phase ($\chi_a = N_a - L_a + O_a$, where N_a is the number of isolated units, L_a is the number of redundant loops, and O_a is cavities with $O_a = 0$

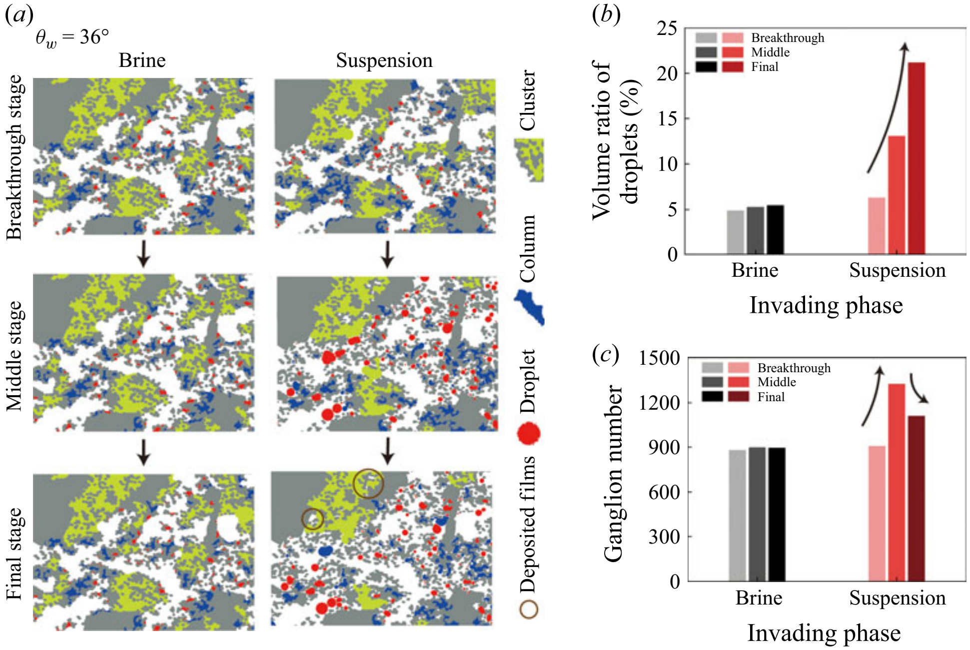

Figure 3. Wetting-film development and residual NAPL detachment induced by nanoparticle adsorption. (*a*) Local view of topological characteristics of the residual non-aqueous phase. (*b,c*) Evolution of (*b*) volume ratio of droplets and (*c*) ganglion number during injection of brine and nanoparticle suspensions. The middle stage corresponds to half the duration of the final stage.

for 2D topology) reflects more connected invasion networks by nanoparticle-induced wettability variation.

To identify the displacement pattern controlled by nanoparticles, topological features under the moderately water-wet condition were quantified and compared. Based on the Euler number χ_n (calculated per ganglion), residual NAPL was categorised into isolated ganglia ($\chi_n = 1$) and clusters ($\chi_n < 1$). Using the shape factor $c_n = 4\pi A_n / p_n^2$ (A_n is the area and p_n is the perimeter), isolated ganglia were further classified as droplets ($c_n \geq 0.5$) or columns ($c_n < 0.5$). As shown in figure 3, when initial mainstream paths were established at breakthrough, the phase distribution, droplet ratio and ganglion number were close for brine and suspension displacement. After breakthrough, phase topology showed negligible change for brine due to relatively weak film flow. In contrast, suspension injection generated large amounts of droplets at the post-breakthrough stage, indicating continuous detachment of residual NAPL. Droplet formation was driven by enhanced wetting-film development, which was visible even in deep stagnant zones occupied by NAPL (figure 3*a*). The monotonically increasing trend of the droplet ratio (figure 3*b*) aligns with pore-scale observations, while fluctuations in the ganglion number (figure 3*c*) indicate that droplets were not only peeled off but also mobilised. These results suggest that nanoparticle-induced wettability variation occurs after the establishment of mainstream paths at breakthrough, thus free of the negative effects associated with strongly water-wet states (Lei *et al.* 2023).

As discussed in § 3.1, spontaneous formation of wetting films driven by corner flow is essential for nanoparticle effect on wettability, while the shift toward stronger hydrophilicity induced by particle adsorption (corresponding to a transition from state IV to state III as depicted in figure 1*d*) promotes aqueous film growth and enables detachment of NAPL droplets. The difference in film development can be qualitatively assessed using theoretical models for corner flow (Dong & Chatzis 1995), which give the film flow rate in a square channel as $Q_f = aC(2K)^{-1/2}(\sigma/\mu\beta)^{1/2}R^{5/2}t^{-1/2}$, where a and K are semi-analytical coefficients, $C = 4[\cos\theta\cos(\pi/4+\theta)/\sin(\pi/4) - (\pi/4-\theta)]$ is the shape factor, β is the dimensionless flow resistance also dependent on θ (Ransohoff & Radke 1988), $R = D_h[\cos\theta - \sqrt{\pi/4-\theta+\sin\theta\cos\theta}]/[2(\theta-\pi/4)+2\cos^2\theta - 2\sin\theta\cos\theta]$ is the curvature radius of corner-film meniscus, D_h is the hydraulic diameter, and t is the characteristic time. Accordingly, the wettability dependence can be expressed as $Q_f \propto C(\theta)[\beta(\theta)]^{-1/2}[R(\theta)]^{5/2}$. Assuming effective wettability alteration as in static NAPL droplet systems (from $\theta_w \approx 36^\circ$ to $\theta_{eff} \approx 15^\circ$), we obtain $Q_{f,NP}/Q_{f,0} \approx 16$, where the subscripts NP and 0 denote nanoparticle-modified and unmodified conditions, respectively, indicating that film accumulation efficiency on nanoparticle-modified surfaces can be over an order of magnitude higher than that on unmodified surfaces. Moreover, tortuous pore spaces in disordered media can induce more complex film transport. As discussed in our previous work (Lei *et al.* 2025), nanoscale roughness from adsorbed particles stabilises wetting films against convex geometries, further amplifying the difference. Note that the effective wettability in pore space may differ from the intrinsic value in state characterisations due to hysteresis effects from surface roughness, dynamic effects during displacement, mixed wettability and so on (Lin *et al.* 2019; Sun *et al.* 2020). Nevertheless, the generality of our wettability criterion remains valid, as it depends on the intrinsic property of the substrate.

3.3. *Generality of the wettability criterion with structural hierarchy effects*

We further conducted displacement experiments in designed disordered media with varying degrees of structural hierarchy. The pore size distribution progressively evolved from a long-tailed form in the strongly hierarchical structure to a nearly Gaussian form in the weakly hierarchical one (figure 4*a*). Single-phase network modelling was performed not to exactly reproduce the phase and velocity distributions under two-phase conditions, but to provide statistical information on intrinsic structural properties based on segmented pore–throat units (see the supporting information for details). The structural heterogeneity factor is defined as $CV_s = \sqrt{\langle (D-D_m)^2\rangle_V}/D_m$, where D is the local pore diameter, D_m is the mean pore diameter, and $\langle\rangle_V$ denotes volume-weighted averaging. The flow heterogeneity factor is similarly defined as $CV_f = \sqrt{\langle (U-U_m)^2\rangle_q}/U_m$, where U is the local throat velocity, U_m is the injection velocity (identical for all structures), and $\langle\rangle_q$ denotes weighting by local flow rate. As presented in figure 4(*b*), CV_f exhibits a super-linear dependence on CV_s, highlighting the sensitivity of flow heterogeneity to structural hierarchy.

Figure 4(*c*) shows the relative displacement performance of nanoparticle suspensions compared with brine. The wettability criterion ($\theta_w < \theta_{w,cr}$) holds across all tested structures, exhibiting a consistent transition from negligible to significant increase in S_a at the final stage with increasing substrate hydrophilicity. Nevertheless, nanoparticle-induced improvement in efficiency under the effective condition weakened as the structure became more uniform. Variations in droplet ratio (figure 4*d*) followed the same trend as displacement efficiency, indicating similar mechanisms as presented in figure 3.

To probe the link between structural features and flow patterns, local phase distributions in experiments are compared with flow fields from single-phase lattice Boltzmann simulations (figure 4*e*; see the supporting information for detailed discussion on two-phase simulations). Fingering pathways during brine displacement largely coincided with

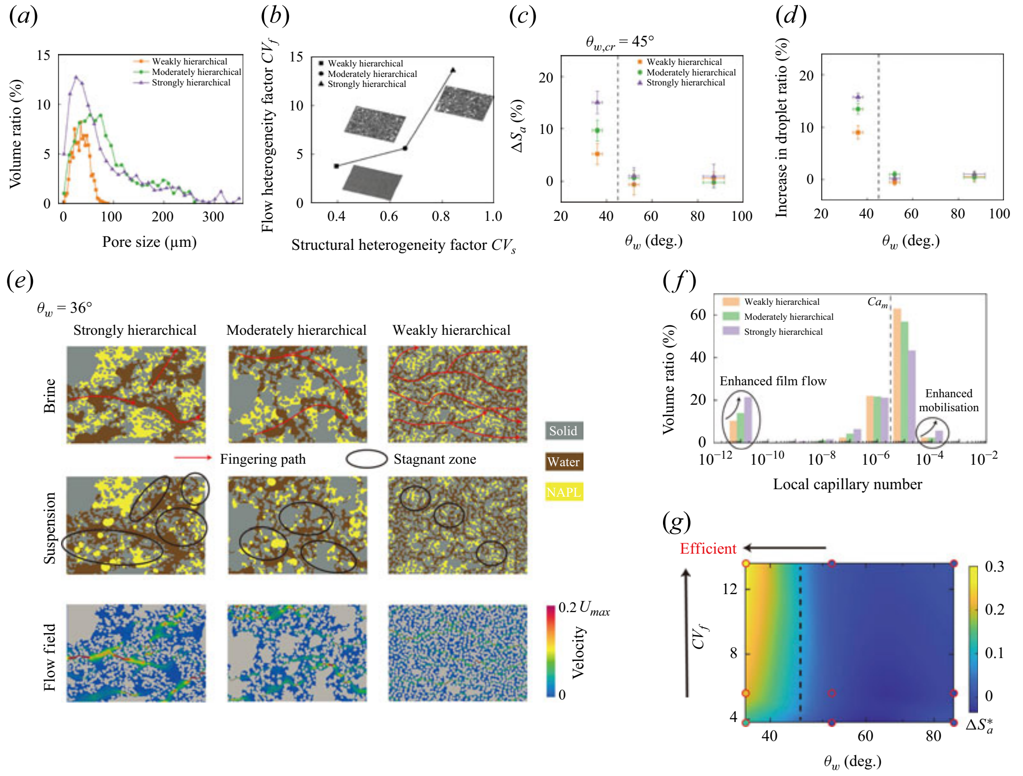

Figure 4. Coupled effects of wettability and structural properties on nanoparticle behaviour during multiphase displacement. (*a*) Variation in the pore size distribution from strongly to weakly hierarchical disordered media. (*b*) Relationship between the structural heterogeneity factor CV_s and flow heterogeneity factor CV_f. Insets show schematics of the structures. (*c,d*) Variations in (*c*) relative displacement performance ΔS_a (difference between S_a of suspension and brine) and (*d*) droplet ratio increase at the final stage for different structures in microfluidic experiments. (*e*) Local views of phase distributions from experiments and flow fields from lattice Boltzmann simulations. (*f*) Distribution of the local capillary number $Ca_i = \mu U_i/\sigma$ defined on throat unit i, with U_i from network simulations. The leftmost columns include Ca_i down to zero, and Ca_m denotes the global characteristic capillary number. (*g*) Illustrative phase diagram showing coupled effects of structural and wettability properties on nanoparticle-enhanced displacement, where $\Delta S_a^* = \Delta S_a/S_{a,0}$ and $S_{a,0}$ denotes the final aqueous phase saturation in brine displacement. Each circle represents the average of three sets of independent experiments.

the high-speed channels. Instead, detachment of residual NAPL by nanoparticles occurred primarily in low-speed stagnant zones, where a low local capillary number suppresses the main meniscus flow and allows wetting films to develop fully (Lei *et al.* 2023). The higher local capillary number in preferential paths enables ganglion mobilisation under stronger viscous forces (Datta, Ramakrishnan & Weitz 2014), producing a synergistic effect. By defining $Ca_i = \mu U_i/\sigma$ for each throat unit i, statistics in figure 4(*f*) show that with increasing structural hierarchy, the volume fractions of regions with extremely low Ca_i ($< 10^{-10}$) that benefit film flow and high Ca_i ($> 10^{-4}$) that mobilise ganglia both increase, accounting for the enhanced displacement.

Figure 4(*g*) summarises these findings in an illustrative phase diagram, where the displacement behaviour of nanoparticle suspensions is governed by the interplay between wettability and structural conditions. Constrained by substrate wettability (satisfying the corner-flow criterion) and modulated by structural hierarchy, nanoparticle-induced displacement enhancement is more efficient in hydrophilic media with stronger flow heterogeneity. This is consistent with qualitative trends in the literature: on the one hand, the reported displacement enhancement was generally stronger under more hydrophilic conditions (Zhang *et al.* 2018; Mohammadalinejad *et al.* 2019). On the other hand, variations in the extent of improvement among different types of porous media (Zhang *et al.* 2016; Li *et al.* 2017; Lu & Wang 2023) may be explained by structural hierarchy effects, as a more random structure typically exhibits a stronger hierarchy and flow heterogeneity, thereby amplifying nanoparticle effects. Although the proposed mechanisms are theoretically general, 3D effects arising from increased topological connectivity and spatial complexity in natural porous media should be carefully considered for engineering applications, as they may strengthen film flow and increase the sensitivity to wettability and structural properties.

4. Conclusion

In summary, we establish mechanistic criteria for nanoparticle-induced wettability alteration in multiphase flow systems via multiscale experiments, theoretical derivations and simulations. By linking interfacial wetting states with pore-scale displacement patterns, we show that nanoparticle adsorption reshapes displacement only when corner flow enables film spreading. Enhanced development of wetting films and mobilisation of residual non-aqueous droplets account for the improved displacement under conditions satisfying the wettability criterion. While the criterion holds generally across varying disordered media, the degree of structural hierarchy modulates the magnitude of displacement enhancement by variations in flow heterogeneity. Our findings elucidate how wettability and structural properties jointly control nanoparticle behaviour and multiphase displacement, offering guidance for rational design of nanoparticle-based strategies for flow control in disordered media.

Supplementary material. Supplementary material is available at https://doi.org/10.1017/jfm.2026.11308.

Funding. This work is financially supported by the NSF grants of China (nos 12432013, U24B6003, 12272207).

Declaration of interests. The authors report no conflict of interest.

Author contributions. M.W. designed the research and supervised the project; X.L., M.Z., Y.Y. and T.J. performed the experimental research; X.L. and Y.L. performed the numerical research; X.L., M.Z. and W.L. analysed data; X.L. and M.W. prepared the paper with feedback from all authors.

REFERENCES

AL-ANSSARI, S., BARIFCANI, A., WANG, S., MAXIM, L. & IGLAUER, S. 2016 Wettability alteration of oil-wet carbonate by silica nanofluid. *J. Colloid Interface Sci.* **461**, 435–442.

ALZOBAIDI, S., WU, P.K., DA, C., ZHANG, X., HACKBARTH, J., ANGELES, T., RABAT-TORKI, N.J., MACAULIFFE, S., PANJA, S. & JOHNSTON, K.P. 2021 Effect of surface chemistry of silica nanoparticles on contact angle of oil on calcite surfaces in concentrated brine with divalent ions. *J. Colloid Interface Sci.* **581**, 656–668.

BLUNT, M.J. 2017 *Multiphase Flow in Permeable Media: A Pore-Scale Perspective*. Cambridge University Press.

BROWNE, C.A., HUANG, R.B., ZHENG, C.W. & DATTA, S.S. 2023 Homogenizing fluid transport in stratified porous media using an elastic flow instability. *J. Fluid Mech.* **963**, A30.

CONCUS, P. & FINN, R. 1969 On the behavior of a capillary surface in a wedge. *Proc. Natl Acad. Sci. USA* **63** (2), 292–299.

DATTA, S.S., RAMAKRISHNAN, T.S. & WEITZ, D.A. 2014 Mobilization of a trapped non-wetting fluid from a three-dimensional porous medium. *Phys. Fluids* **26** (2), 022002.

DONG, M. & CHATZIS, I. 1995 The imbibition and flow of a wetting liquid along the corners of a square capillary tube. *J. Colloid Interface Sci.* **172** (2), 278–288.

DUDUKOVIC, N.A., FONG, E.J., GEMEDA, H.B., DEOTTE, J.R., CERÓN, M.R., MORAN, B.D., DAVIS, J.T., BAKER, S.E. & DUOSS, E.B. 2021 Cellular fluidics. *Nature* **595** (7865), 58–65.

HUPPERT, H.E. & NEUFELD, J.A. 2014 The fluid mechanics of carbon dioxide sequestration. *Annu. Rev. Fluid Mech.* **46** (1), 255–272.

LEI, W., LU, X., GONG, W. & WANG, M. 2023 Triggering interfacial instabilities during forced imbibition by adjusting the aspect ratio in depth-variable microfluidic porous media. *Proc. Natl Acad. Sci. USA* **120** (50), e2310584120.

LEI, W., LU, X., YANG, G., BAGHERI, S. & WANG, M. 2025 Reverse capillary trapping and self-removal of non-aqueous fluid from dead-end structures by nanoparticle suspension. *J. Fluid Mech.* **1009**, A14.

LI, R., JIANG, P., GAO, C., HUANG, F., XU, R. & CHEN, X. 2017 Experimental investigation of silica-based nanofluid enhanced oil recovery: the effect of wettability alteration. *Energy Fuels* **31** (1), 188–197.

LIM, S., HORIUCHI, H., NIKOLOV, A.D. & WASAN, D. 2015 Nanofluids alter the surface wettability of solids. *Langmuir* **31** (21), 5827–5835.

LIN, Q., BIJELJIC, B., BERG, S., PINI, R., BLUNT, M.J. & KREVOR, S. 2019 Minimal surfaces in porous media: pore-scale imaging of multiphase flow in an altered-wettability bentheimer sandstone. *Phys. Rev. E* **99** (6), 063105.

LIU, Y., GONG, W., ZHAO, Y., JIN, X. & WANG, M. 2022 A pore-throat segmentation method based on local hydraulic resistance equivalence for pore-network modeling. *Water Resour. Res.* **58** (12), e2022WR033142.

LU, X. & WANG, M. 2023 Shape and surface property effects on displacement enhancement by nanoparticles. *Intl J. Mech. Sci.* **255**, 108471.

MOHAMMADALINEJAD, P., HOSSEINPOUR, N., RAHMATI, N. & RASAEI, M.R. 2019 Formation damage during oil displacement by aqueous sio2 nanofluids in water-wet/oil-wet glass micromodel porous media. *J. Petrol. Sci. Engng* **182**, 106297.

PAK, T., LUZ, L.F.DEL., TOSCO, T., COSTA, G.S.R., ROSA, P.R.R. & ARCHILHA, N.L. 2020 Pore-scale investigation of the use of reactive nanoparticles for in situ remediation of contaminated groundwater source. *Proc. Natl Acad. Sci. USA* **117** (24), 13366–13373.

QIN, F., FEI, L., ZHAO, J., KANG, Q., DEROME, D. & CARMELIET, J. 2023 Lattice Boltzmann modelling of colloidal suspensions drying in porous media accounting for local nanoparticle effects. *J. Fluid Mech.* **963**, A26.

QUÉRÉ, D. 2008 Wetting and roughness. *Annu. Rev. Mater. Res.* **38** (1), 71–99.

RANSOHOFF, T.C. & RADKE, C.J. 1988 Laminar flow of a wetting liquid along the corners of a predominantly gas-occupied noncircular pore. *J. Colloid Interface Sci.* **121** (2), 392–401.

SHARDT, N. & ELLIOTT, J.A.W. 2020 Gibbsian thermodynamics of Wenzel wetting (was Wenzel wrong? revisited). *Langmuir* **36** (1), 435–446.

SUN, C., MCCLURE, J.E., MOSTAGHIMI, P., HERRING, A.L., BERG, S. & ARMSTRONG, R.T. 2020 Probing effective wetting in subsurface systems. *Geophys. Res. Lett.* **47** (5), e2019GL086151.

SUNDIN, J. & BAGHERI, S. 2022 Slip of submerged two-dimensional liquid-infused surfaces in the presence of surfactants. *J. Fluid Mech.* **950**, A35.

WANG, M., WANG, J., PAN, N. & CHEN, S. 2007 Mesoscopic predictions of the effective thermal conductivity for microscale random porous media. *Phys. Rev. E* **75** (3), 036702.

WASAN, D.T. & NIKOLOV, A.D. 2003 Spreading of nanofluids on solids. *Nature* **423** (6936), 156–159.

WONG, P.-Z., KOPLIK, J. & TOMANIC, J.P. 1984 Conductivity and permeability of rocks. *Phys. Rev. B* **30** (11), 6606–6614.

XU, K., ZHU, P., COLON, T., HUH, C. & BALHOFF, M. 2017 A microfluidic investigation of the synergistic effect of nanoparticles and surfactants in macro-emulsion-based enhanced oil recovery. *SPE J.* **22** (02), 459–469.

ZHANG, H., RAMAKRISHNAN, T.S., NIKOLOV, A. & WASAN, D. 2016 Enhanced oil recovery driven by nanofilm structural disjoining pressure: flooding experiments and microvisualization. *Energy Fuels* **30** (4), 2771–2779.

ZHANG, H., RAMAKRISHNAN, T.S., NIKOLOV, A. & WASAN, D. 2018 Enhanced oil displacement by nanofluid's structural disjoining pressure in model fractured porous media. *J. Colloid Interface Sci.* **511**, 48–56.

ZHAO, B., MACMINN, C.W. & JUANES, R. 2016 Wettability control on multiphase flow in patterned microfluidics. *Proc. Natl Acad. Sci. USA* **113** (37), 10251.